LUND UNIVERSITY
Faculty of Science

Pulse Compression of Short Wave Infrared Optical Parametric Amplified Pulses using a Hollow Core Capillary

Neven Ibrakovic

LRAP-504
Thesis submitted for the degree of Master of Science
Project duration: 13 months
Supervised by Esben Witting Larsen and Johan Mauritsson

Department of Physics
Division of Atomic Physics
May 2015

Abstract

In this thesis, a method for producing few-cycle short wavelength infrared pulses is presented. The pulses are created by down converting the 800 nm output of a Ti:Sapphire laser in an optical parametric amplifier to 1300 nm, and spectrally broadened in a hollow core fiber in order to obtain a short transform limited pulse duration. Further, they are to be compressed using the anomalous dispersion of a potassium dihydrogen phostphate crystal. The aim of the compression is to generate few cycle pulses in the short wave infrared regime for future high-order harmonic generation experiments. By increasing the wavelength, the energy of the harmonics will be increased, which would allow for new kinds of experiments to be conducted. The pulses have been successfully broadened to support a four cycle duration, however, compression of the pulses remains to be done.

Contents

Acronyms

DFG Difference Frequency Generation.

FWHM Full Width at Half Max.

FWM Four Wave Mixing.

GDD Group Delay Dispersion.

GVD Group Velocity Dispersion.

HCF Hollow Core Fiber.

HHG High-Order Harmonic Generation.

KDP Potassium Dihydrogen Phosphate.

NIR Near Infrared.

OPA Optical Parametric Amplifier.

SPM Self Phase Modulation.

TOD Third Order Dispersion.

XUV Extreme Ultraviolet.

1 Introduction

1.1 Outline of the Thesis

This thesis is segmented into 4 sections. In the introduction section in Sec.1. the aim and the background will be elaborated on. The semi-classical three step model for High-Order Harmonic Generation (HHG) will be properly introduced and its wavelength dependence will be explained and spectral broadening and compression of pulses will be briefly introduced.

Following the introduction, the method for the experiment is described in Sec. 2. In Sec. 2.1. we properly describe dispersion and how it influences pulse duration, and the nonlinear effects that cause spectral broadening in gases. In Sec. 2.2 the design for the setup to spectrally broaden the laser pulses is presented. In Sec. 2.3 the laser source for the setup is introduced, and means of efficiently coupling of the laser into the capillary is motivated.

The results for three experiments are presented and discussed in Sec. 3. Sec. 4 contains the summary of the results obtained and a discussion regarding how well the aim of the thesis is met. The same section contains an outlook which describes possible improvements to the setup and future characterization of the compressed pulses.

1.2 Aim and Procedure

The goal of this study is to create few-cycle pulses in the short wavelength infrared regime. The output from an Optical Parametric Amplifier (OPA) is to be spectrally broadened by propagating the pulses through a Hollow Core Fiber (HCF) filled with a noble gas. The idler of this kind of OPA, a He-TOPAS-Prime [1], has previously been spectrally broadened in a HCF and compressed using anomalous dispersion of fused silica at 1800 nm [2]. However, it is possible to spectrally broaden the output signal aswell, and we propose a new way of compressing the pulses by using the anomalous dispersion of a Potassium Dihydrogen Phosphate (KDP) crystal at down to a 1300 nm central wavelength (also called the carrier wavelength).

In order to meet the final goal a qualitative analysis is performed, where we base the design of the planned setup on an existing setup intended for compressing the output of a Ti:Sapphire, 1 KHz repetition rate laser system which produces 5 mJ, 20 femtosecond (10^{-15} s) pulses centered at 800 nm. The wavelength supercontinuum generated in helium with this setup ranges from 450-1000 nm, which is sufficient to compress a pulse to a single optical cycle at 800 nm, and pulse

durations of approximately 3 fs are obtained.

The same Ti:Sapphire laser is used to pump the TOPAS in order to produce a signal output centered at 1300 nm with up to 0.8 mJ of pulse energy. Accounting for the differences in pulse energy and carrier wavelength of the two sources it is possible to determine a suitable HCF and design a pressure chamber to house it, with the aim of achieving spectral broadening in argon. The challenge is to efficiently broaden relatively low energy pulses using Self Phase Modulation (SPM) (which usually requires high intensities) without loosing too much energy due to ionization and waveguide attenuation.

The compressed pulses should in the end have enough intensity for HHG experiments. The benefit of constructing such a setup would be the possibility of obtaining higher energy of the harmonics, and shorter duration of the generated attosecond (10^{-18} s) pulses. Since at low wavelengths, the electrons accumulate more ponderomotive energy during the acceleration phase in the three step model. Additionally, the rate of direct ionization is reduced as the photon energies are smaller.

1.3 Background

Time-resolved spectroscopy has long been a field within atomic physics, with a history preceding even the invention of the laser [3, 4]. With the invention of Q-switching [5] and laser mode locking [6] it became possible to generate nanosecond (10^{-9} s), and later also down to femtosecond pulses. In order to resolve an event it is necessary that the pulse duration is at least on the same order of magnitude as the duration of the event.

One of the historical milestones of time-resolved laser spectroscopy was the birth of femtochemistry [7], where it became possible to determine molecular dynamics using femtosecond pulses, for which Ahmed Zewail was awarded with the Nobel prize in physics in 1999 [8]. In order to resolve the electron dynamics in an atom, the femtosecond regime is not sufficient since electron dynamics occur on a much shorter timescale. To resolve electron processes in atoms and molecules it is required to use attosecond pulse durations, which can not be obtained using conventional mode-locking and Q-switching techniques.

It is instructive to consider the fundamental restrictions of pulse duration. Firstly, a propagating pulse can not be shorter than a single optical cycle of the carrier wavelength. A single cycle is defined as the time it takes the carrier wavelength to oscillate once. Secondly, a pulse can not be shorter than the Fourier transform of its frequency spectrum. The transform limited duration of a pulse is given by:

$$\tau = \frac{0.44}{\Delta\nu}, \tag{1}$$

where the pulse duration τ is inversely proportional to the frequency bandwidth $\Delta\nu$. The factor 0.44 in Eq. 1 implies that the pulse is Gaussian in time and frequency.

For a long time the shortest pulse duration was limited to the femtosecond regime (the single cycle duration of visible and infrared light), and it was not until the demonstration of HHG [9, 10] that the possibility to obtain pulses with attosecond duration opened up. The Extreme Ultraviolet (XUV) radiation created by HHG is ideal for short pulses, as the single cycle duration is very short compared to the infrared and visible light provided by solid state lasers, and it comes with a large bandwidth, allowing for a short Fourier transform limit of the pulses. However, a method of measuring the attosecond pulses was not demonstrated until 2001 [11].

Today, high-order harmonics are generally generated at the Department of Atomic Physics in Lund using 800 nm laser pulses. The motivation for this thesis is future HHG experiments generated with a longer wavelength of the driving laser.

1.4 High-Order Harmonic Generation

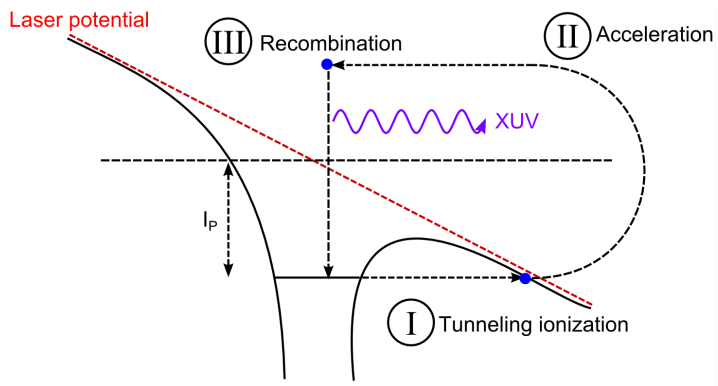

Figure 1: Illustration of the HHG semiclassical three step process.

HHG can be described by a semiclassical three step process, as seen in Fig. 1 [12]:

I An atom is subjugated to a strong laser field that distorts the atomic potential so that tunneling ionization occurs.

II The electron is accelerated away from the atom.

III The electric field changes direction and the electron is accelerated back into the parent ion where it may recombine. In the event of recombination, the excess energy is released in the form of an energetic XUV photon.

The tunneling ionization can occur at different times during a laser cycle. Meaning that the electrons accumulate different amounts of kinetic energy during the acceleration phase. This leads to the generation of a broadband spectrum containing many energies for the different trajectories. Due to the symmetry of the laser field, HHG occurs twice per optical cycle. In the frequency domain this corresponds to a frequency separation that is two times the carrier frequency. This process gives rise to the characteristic HHG spectrum containing a plateau of frequency peaks, as shown in Fig. 2 ranging from harmonics $\sim 7 - 30$. Following the plateau is a steep decrease in intensity, called the harmonic "cutoff" [15]. The cutoff energy is the highest possible energy of the harmonics, and is classically given by:

$$E_c = I_p + 3.17U_p, \tag{2}$$

where I_p is the ionization potential of the atom and U_p is the ponderomotive energy, the average oscillation energy that the electrons acquire during the laser

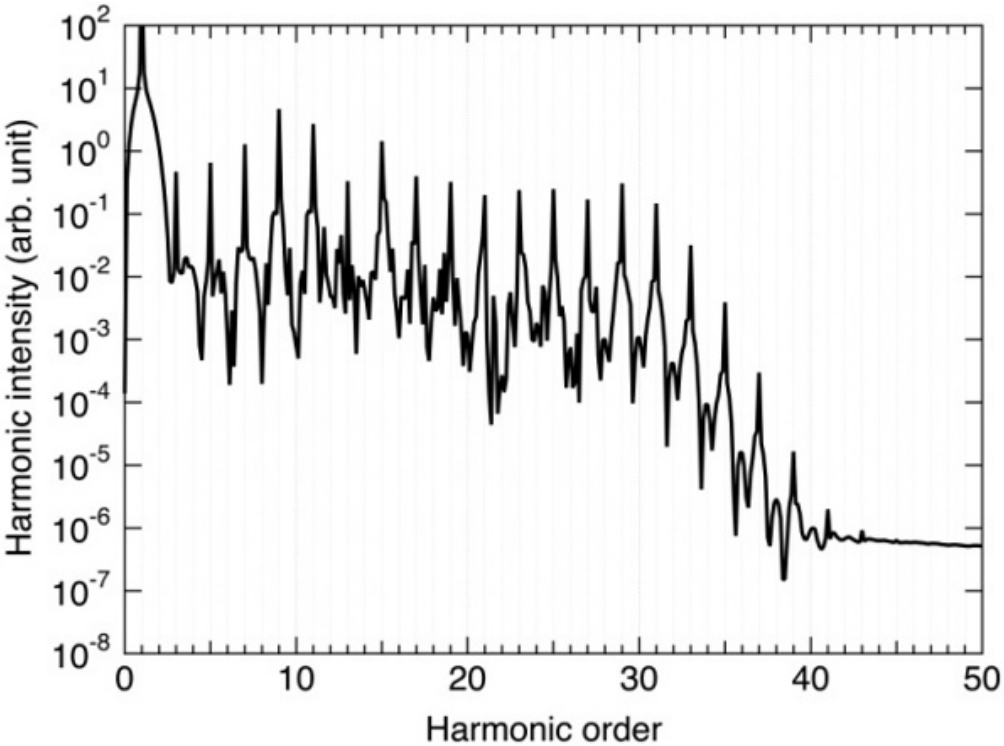

Figure 2: Simulation of a typical HHG spectrum. Retrieved from [13].

field. The ponderomotive energy is proportional to the square of the driving field wavelength λ [14]:

$$U_p = 9.33 \cdot 10^{-14} I \lambda^2 [eV], \tag{3}$$

where λ is the wavelength in μm and I is the intensity in W/cm^2. It is therefore possible to generate higher harmonic energies when using longer driving wavelength [16]. To produce longer wavelengths in the experiments described in this thesis, we down-convert the 800 nm laser output using an OPA to short wavelength infrared.

While the cutoff scales favorably with longer wavelength, the harmonic yield unfortunately scales as $\sim \lambda^{-6}$ [17], which quickly leads to low or no yield when increasing the wavelength for a fixed laser intensity. Meaning that there is a compromise between harmonic energy and the pure yield of the harmonics, and this motivates our choice of carrier frequency. Since a carrier wavelength that is close to the mid-IR might not generate high-order harmonics at all without further amplifying our laser.

1.5 Pulse Compression

The HHG process requires a laser driving field with a high intensity, as the electric field of the pulses has to compete with the Coulomb potential that the electron experiences in order to obtain tunneling ionization. High intensity is achieved by focusing ultrashort pulses on the gas target. Normally, the driving field used to generate high-order harmonics is required to be in the femtosecond regime, which requires a large bandwidth in order to ensure a short pulse duration. When down-converting the pulses without any amplification, short pulse duration might be extra important, since the available energy is reduced in the conversion process.

In order to compress the pulses it is necessary to spectrally broaden to achieve a shorter transform limit of the pulse duration. Spectral broadening in our case is achieved by SPM in an HCF filled with argon. The HCF acts as an waveguide and confines the beam within a small area over a long distance, as high intensity is required for SPM. It would also be possible to spectrally broaden pulses in crystals and glasses, however, high energy pulses are likely to damage solid materials, whereas gas can not be damaged in that sense.

The process of spectral broadening often leads to a temporal broadening as well. This is mainly due to that the frequency components travel at different velocities in the optical elements, known as "dispersion". When a propagating pulse accumulates dispersion it is said to be "chirped", and removal of this chirp effectively compresses the pulse again.

At 800 nm chirped mirrors can be used to compress a pulse [18], these are however more difficult to produce for the short wavelength infrared region, and the design of such is a research project in itself. However, in the short wavelength infrared region most materials have anomalous dispersion, *i.e.* blue travels faster than red, and can therefore effectively compress the pulses which have accumulated normal dispersion. The shift from normal to anomalous dispersion occurs near 1300-1500 nm for most materials. KDP is of special interest, since it has anomalous dispersion starting from around 1000 nm and previous simulations show that pulse compression in KDP should be achievable for carrier wavelengths down to 1040 nm [19]. Although this still remains experimentally unconfirmed.

2 Method

2.1 Theoretical Considerations

2.1.1 Dispersion

Dispersion is a fundamental feature in all materials. In Fig. 3 the refractive index as a function of wavelength is presented, and it becomes apparent that for a broadband pulse, the various wavelength components will propagate at different speeds through the medium and acquire different delays once transmitted.

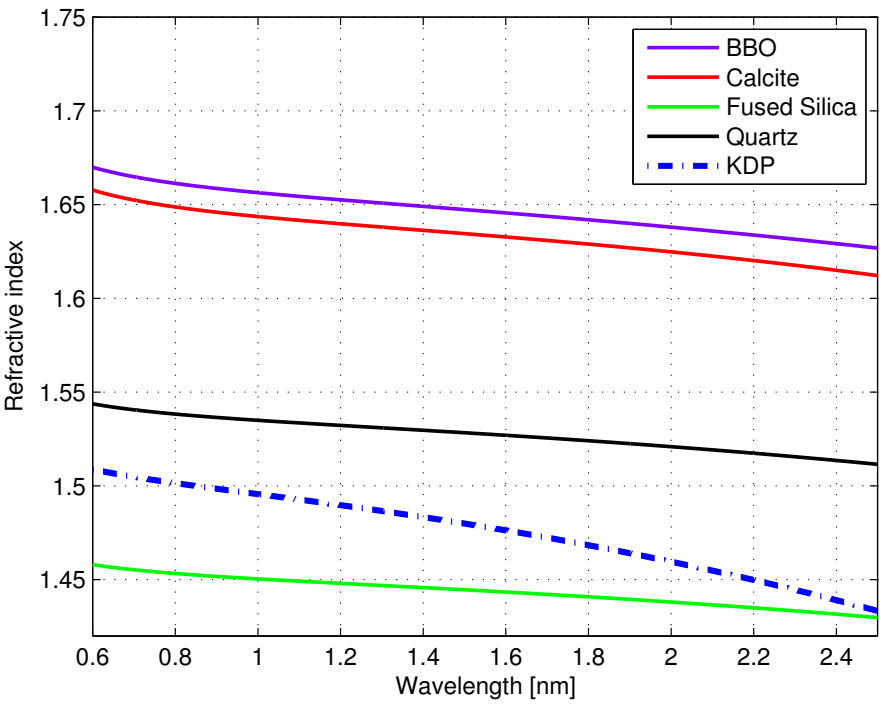

Figure 3: The refractive index for an assortment of materials used in the setup.

The pulse will therefore become chirped after it has passed through the material. To first order approximation this chirp can be described by the Group Velocity Dispersion (GVD) parameter β [20]:

$$\beta = \frac{\delta^2 k}{\delta \omega^2} = \frac{\lambda_0^3}{2\pi c_0^2} \frac{\delta^2 n}{\delta \lambda_0^2}, \tag{4}$$

where k is the wave vector and ω is the angular frequency of the pulse. In the

right hand term of Eq. 4, GVD is represented as a function of wavelength, λ_0 and refractive index n. This expression is useful since it makes it possible to calculate GVD using the Sellmeier equation for different materials. The Sellmeier equations are empirically fitted formulas, which provide a good analytic approximation of the wavelength dependent refractive index [21].

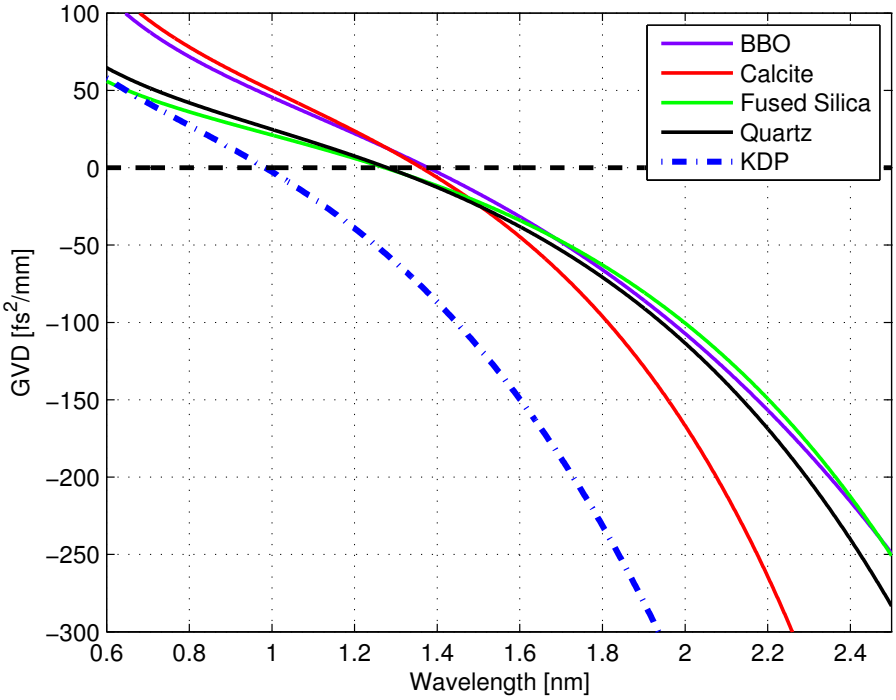

Figure 4: The group velocity dispersion (GVD) for a number of materials relevant to this thesis work.

Fig. 4 shows the GVD as a function of wavelength for different materials. It is worth to mention that GVD is in the frequency domain an additive quantity. Positive dispersion (normal dispersion) means that high energy photons have lower group velocity than low energy photons and negative dispersion (anomalous dispersion) means the exact opposite. This means that in theory, GVD acquired in *e.g.* calcite can be removed with KDP for a pulse with 1300 nm carrier wavelength.

It has previously been presented by Schmidt and coworkers [2] that it is possible to compress ultrashort pulses using anomalous dispersion of fused silica at 1800 nm, similar compression technique for 1300 nm carrier wavelengths should be possible using KDP. The required bandwidth for a transform limited pulse to achieve single cycle duration at 1300 nm is around 600 nm. This entire band-

width could, from looking at these calculations, be compressed using KDP.

As GVD is evaluated at the center wavelength it assumes that there is a linear phase contribution across the bandwidth of the pulse spectrum. This is sufficient for narrow bandwidths as a short distance on the GVD curve might well be approximated by the tangent in one point. For larger bandwidths however, this is not true and also the Third Order Dispersion (TOD) has to be calculated and accounted for. The TOD can be expressed as:

$$\beta' = \frac{\delta}{\delta\omega}\beta = -\frac{\lambda^2}{2\pi c_0}\frac{\delta}{\delta\lambda}\beta. \tag{5}$$

As GVD is a good measure of uniform pulse broadening, the quadratic phase contribution from TOD quantifies the non-uniform pulse broadening, which distorts the pulse shape [22]. Fig. 5 shows TOD as a function of wavelength for different materials. Since the TOD does not become negative at any given point it is impossible to remove the quadratic phase contributions using only material dispersion properties.

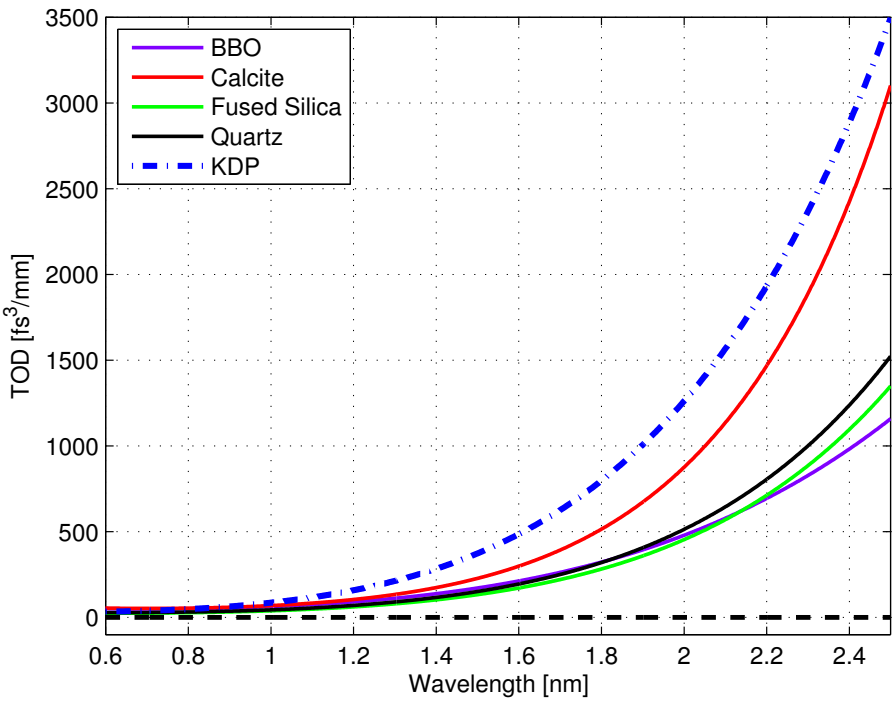

Figure 5: The third order dispersion (TOD) for an assortment of materials.

The Group Delay Dispersion (GDD) is the product of the GVD and the thick-

nesses of the materials. This quantity shows how much second order dispersion the pulse obtains when propagating through the optical elements in the setup, and from this it is possible to estimate the required amount of KDP in order to compress the pulse. Given that the thickness of the KDP is calculated, the amount of TOD acquired in all the optical elements can be estimated.

Material	Thickness [mm]	GDD [fs^2]	TOD [fs^3]
Air	8000	101.9	72.6
Argon	2000	12.5	8.8
Fused silica	5	-11.4	394.6
KDP	1.68	-102.9	357.5

Table 1: Second and third order dispersion obtained from the materials in the setup for a pulse with a 1300 nm carrier wavelength.

Table 1 shows an estimation of the materials in the beamline, and the required amount of KDP in order to remove all GDD from the pulse. Also shown is how much TOD is acquired when propagating through all these materials. A contribution of $\sim 800\,\mathrm{fs}^3$ TOD can be considered as a small quantity in order to achieve few cycle pulses, as it has previously been stated that a TOD of $1000\,\mathrm{fs}^3$ does not have a huge impact on the transform limit of $1.8\,\mu$m pulses [2]. It is worth noting that this calculation does not include the nonlinear contribution to the chirp, which arises from high intensity propagation inside the HCF, and estimating this effect requires a split-step simulation of pulse propagation inside a waveguide [23]. It is a time consuming task to construct such an algorithm, and there is no certainty that the result will efficiently predict the accumulated chirp. Thus the assumption is made that $\sim 50\%$ overcompensation in KDP thickness will sufficiently account for nonlinear chirp contributions. Even though fused silica has negative dispersion, it should not be used to compress the pulses, as GVD for fused silica becomes positive near 1300 nm.

2.1.2 Nonlinear Interactions

The spectral broadening of pulses obtained by propagation inside a HCF is the result of nonlinear interaction of an electric field with a medium. At low intensities, we can approximate the polarization density as having a linear relation to the electric field:

$$P(t) = \epsilon_0 \chi E(t), \tag{6}$$

where ϵ_0 is the vacuum permittivity and χ is the electric susceptibility of the medium. However, at high intensities, the response of a medium will be nonlinear. The polarization of the medium must then be expressed as a power series of the applied electric field:

$$P(t) = \epsilon_0 \left[\chi^{(1)} E(t) + \chi^{(2)} E(t)^2 + \chi^{(3)} E(t)^3 + ... \right], \tag{7}$$

where $\chi^{(i)}$ is the ith order susceptibility tensor. However, for a physically meaningful expression for materials that possess inversion symmetry (such as gases, amorphous solids and centrosymmetric crystals), the induced polarization must change sign as the electric field changes sign. This does not occur for the even susceptibility tensors and thus they must equal zero for these materials [24].

Of particular interest is the third order susceptibility tensor which gives rise to Four Wave Mixing (FWM), schematically illustrated in Fig. 6. In the case that this effect is achieved with the photons of one beam it is referred to as SPM, as the beam interacts with itself.

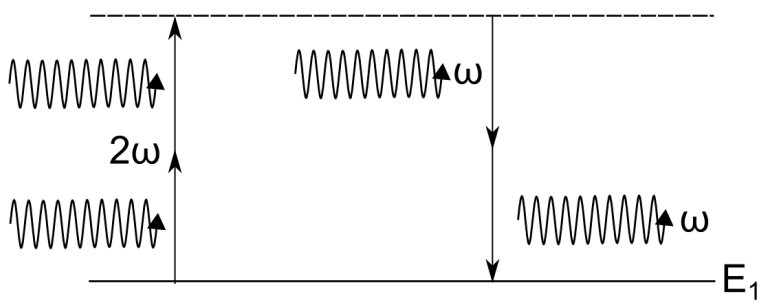

Figure 6: A schematic of FWM. ω is the angular frequency of the photons.

The FWM process can be interpreted as the absorption of two photons to a virtual level followed by an emission of two photons, in the case of Fig. 6, with

the same energy. This might seem as an redundant process in Fig. 6 as it is unmeasurable, since the photon energies and phases are not altered. But what it illustrates is that this is physically allowed, as the conservation of momentum is preserved, or more explicitly that it is phase matched:

$$k_1 + k_2 = k_3 + k_4, \tag{8}$$

as $k_1 = k_2 = k_3 = k_4$. If this process is not fully phase matched, the efficiency will be reduced. For the purpose of broadening the spectrum of a pulse, it is necessary that the generated photons are at different energies than that of the input photons. We can illustrate this effect by assuming that we have a broadband pulse with half-bandwidth Δ, thus we can construct a scenario seen in Fig. 7.

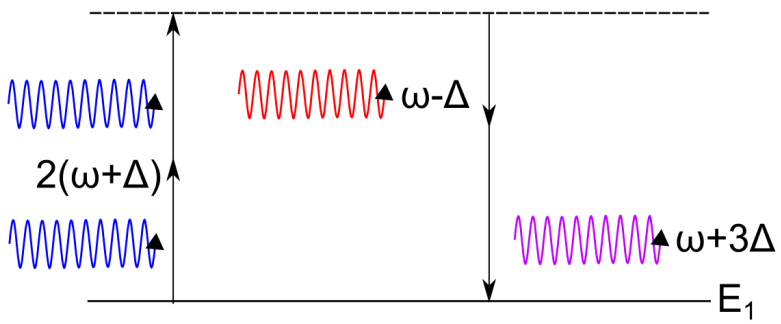

Figure 7: An schematic of FWM using three incident photons in such a way that a maximum photon energy is created for an output photon.

We can describe the efficiency of the conversion process seen in Fig. 7 by looking at the mismatch. We rewrite the wave vector as $k = \frac{\omega \cdot n(\omega)}{c}$ and omit the constants. This allows for the phase matching to be described as:

$$2((\omega + \Delta)n(\omega + \Delta)) - (\omega - \Delta)n(\omega - \Delta) = (\omega + 3\Delta)n(\omega + 3\Delta), \tag{9}$$

where we see that this abides to the energy conservation, but it is only phase matched if the refractive index does not change. The smallest phase mismatch is obtained if the medium has very low dispersion, and low dispersion materials are predominantly gases (as can be seen from the GDD column in Table 1).

This somewhat simplified illustration of FWM however does not explain the emergence of nonlinear chirp that usually is gained from SPM. Therefore we must introduce the phenomena of an intensity dependent refractive index, or

nonlinear refractive index. If the linear refractive index is given by n_0, and the nonlinear index coefficient, n_2, is given by:

$$n_2 = \frac{3\chi^{(3)}}{8n_0}, \tag{10}$$

then the total refractive index, n, can be expressed as:

$$n = n_o + n_2 I(t), \tag{11}$$

where $I(t)$ is the laser pulse intensity [22]. This is called the electro-optic Kerr effect. The presence of a time dependent refractive index introduces a time dependent nonlinear phase shift [25]. The phase of light in a medium is given by:

$$\Phi(z,t) = \omega_0 t - k_0 z n = \omega_0 t - k_0 z(n_0 + n_2 I(t)), \tag{12}$$

where z is propagation length. Then it is possible to obtain the instantaneous frequency as:

$$\omega(t) = \frac{\delta\Phi(z,t)}{\delta t} = \frac{\delta}{\delta t}(\omega_0 t - k_0 z(n + n_2 I(t))). \tag{13}$$

As n_0 is time independent it vanishes, and thus the instantaneous frequency is given by:

$$\omega(t) = \omega_0 - k_0 z n_2 \frac{\delta}{\delta t} I(t), \tag{14}$$

where the right hand term indicates that frequencies other than ω_0 are present. The behavior of the frequency shift in Eq. 14 is basically dependent on the intensity profile in Eq. 11. In order to describe this behavior we omit physical quantities and assume a Gaussian intensity profile. Fig. 8 describes the frequency shift for a Gaussian pulse, the time is expressed in the Full Width at Half Max (FWHM) duration of the pulse. At the leading edge, *i.e.* the front of the pulse, frequencies are red-shifted. The frequency components at the center of the pulse are not shifted and at the trailing edge (back of the pulse) they are blue-shifted. This effect is synonymous to normal dispersion as described in Sec. 2.1.1, meaning that SPM always introduces positive GVD.

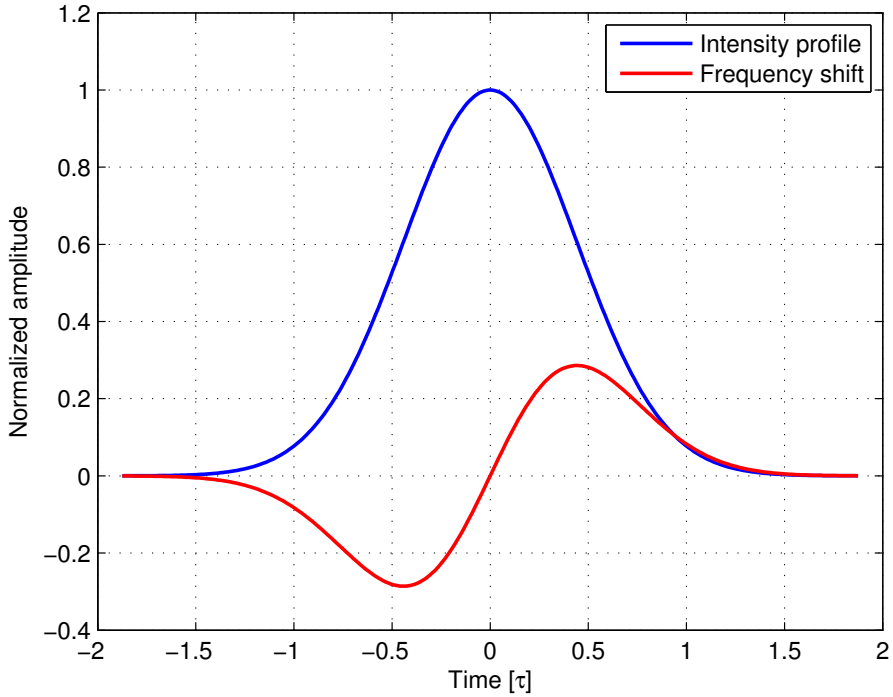

Figure 8: The behavior of nonlinear frequency shift for a Gaussian intensity profile.

2.2 Design Strategy

2.2.1 Choice of a Hollow Core Fiber

In the previous section we explained that in order to achieve spectral broadening it is necessary to have a high intensity. The intensity dependent third order susceptibility, $\chi^{(3)}$, is what facilitates the electro-optic Kerr effect and allows for efficient SPM. Furthermore, in order to have a small phase mismatch of FWM it was deduced that low dispersion materials are best suited for spectral broadening. Additionally, the phase shift introduced from SPM increases with the propagation length, as expressed in Eq. 13.

It is therefore favorable to use a waveguide in order to maintain high intensity over a long propagation length. Propagating through a regular optical fiber with a solid core is not possible due to the high laser intensity, since it will lead to material breakdown. Hence, an approach of propagating in a gas-filled HCF is of more interest for this experiment. This leads to increased waveguide attenuation since the internal reflection, which is the guiding effect in solid core fibers, is replaced with grazing incidence reflection in a HCF.

The HCF will act as a cylindrical waveguide, and one can express the attenuation as [26]:

$$\alpha_{n,m} = \left(\frac{u_{n,m}}{2\pi}\right)^2 \frac{\lambda^2}{a^3} \frac{\frac{1}{2}(\nu^2+1)}{\sqrt{\nu^2-1}}, \tag{15}$$

for a $\mathrm{EH}_{n,m}$ mode. In Eq. 15, $u_{n,m}$ is the Bessel function of n and m, which can be enforced to the lowest possible mode, $u_{1,1}$, as this would provide the smallest contribution to the attenuation constant. ν is the refractive index difference of the core and cladding. The most interesting relation in Eq. 15 is $\frac{\lambda^2}{a^3}$, where λ is the carrier wavelength and a is the core size of the HCF. From this it is apparent that the attenuation decreases rapidly with increasing core size. Which is intuitive if one considers the ray optics interpretation of a waveguide, as rays would reflect more times in a smaller waveguide before they are transmitted. However, an increased core size naturally leads to a reduced intensity, which is one of the important quantities required for SPM.

In order to find a reference for the capillary core size, the 800 nm pulse broadening setup was used as a model for a comparative study. As much of the initial energy is lost in the down-conversion process in the TOPAS it is decided that further waveguide attenuation is undesired. The core for the 1300 nm capillary is thus chosen such that the attenuation constant is the same, or smaller, as for the 800 nm capillary. Using Eq. 15, and assuming that $\nu_{1300} \approx \nu_{800}$, the increase of the attenuation constant is calculated by shifting the carrier wavelength:

$$\frac{\alpha_{1300nm}}{\alpha_{800nm}} \approx \left(\frac{\lambda_{1300}}{\lambda_{800}}\right)^2 \cdot \left(\frac{a_{800}}{a_{1300}}\right)^3 = 2.56 \cdot \left(\frac{a_{800}}{a_{1300}}\right)^3. \tag{16}$$

In order to have the same attenuation constant, the HCF core size has to be increased by a factor of $\sqrt[3]{2.56}$. This corresponds to approximately a 37% increase of the core diameter. As the aperture size of the 800 nm capillary is 250μm a 350μm capillary is chosen (40% larger). This introduces an almost doubled core area, which means that the pulse intensities are halved.

Since at least two thirds of the intensity is lost in the down-conversion process, and half is lost due to the beam size increase, it is necessary to evaluate the strength of the third order polarization density from Eq. 7:

$$P^{(3)} = \chi^{(3)} E(t)^3. \tag{17}$$

This term gives a measure of how strong third order nonlinear effects, such as SPM, are in a medium. Assuming that the intensity has been reduced by a factor of 6, then $P^{(3)}$ in Eq. 17 will be reduced by a factor of $6^{3/2} \approx 15$ compared to the 800 nm setup. If this term is to be equal or larger than in the 1300 nm setup then a gas with larger $\chi^{(3)}$ has to be used.

Fortunately, helium, which is the gas used for spectral broadening in the 800 nm setup, is the atom which has the smallest $\chi^{(3)}$ of the noble gases. The relative third order susceptibilities of neon and argon are [27]:

$$\frac{\chi^3_{Ne}}{\chi^3_{He}} = 1.8, \tag{18}$$

$$\frac{\chi^3_{Ar}}{\chi^3_{He}} = 23.5, \tag{19}$$

evaluated at 1 atmospheric pressure and a wavelength of 1055 nm. This shows that $P^{(3)}$ in the 1300 nm setup can be well compensated by using argon as the medium for SPM.

2.2.2 Capillary Chamber

Figure 9: A SolidWorks rendering of the HCF pressure chamber. The middle connector is detached in order to reveal the internal wire supports of the HCF.

In order to support the HCF and ensure that the high intensity pulses propagate through argon, a pressure chamber is designed. The role of the pressure chamber, shown in Fig. 9, is primarily to provide a straight support for the fiber and confine the noble gas. The chamber should be suitable to both maintaining vacuum and maintaining pressures up to 2-3 Bar, which is achieved by using vacuum tube connectors.

The pressure chamber enables differential pumping, as a blind flange with a small bore hole at its center divides the chamber into two pressure compartments. One high pressure compartment for pumping in gas, and one low pressure compartment for pumping gas out. The HCF is then inserted into the blind flange center bore, which enforces the gas from the high pressure compartment to be pumped out through the capillary. As the pulses are coupled into the fiber in the low pressure compartment, the position of the focus becomes will not be displaced when the pressure is changed. Additionally, coupling into the fiber in high pressure gas might lead to nonlinear effects, such as self-focusing [28], which can drastically reduce the coupling efficiency.

Fig. 10 shows a more detailed schematic of the pressure chamber. Brewster windows are attached to the entrance and exit of the chamber, in order to avoid reflection losses. Two 500 mm straight connectors separate the Brewster windows from the beam focus at the capillary entrance. If the beam spot is too close to the windows, this might introduce nonlinear effects in the glass and in the worst

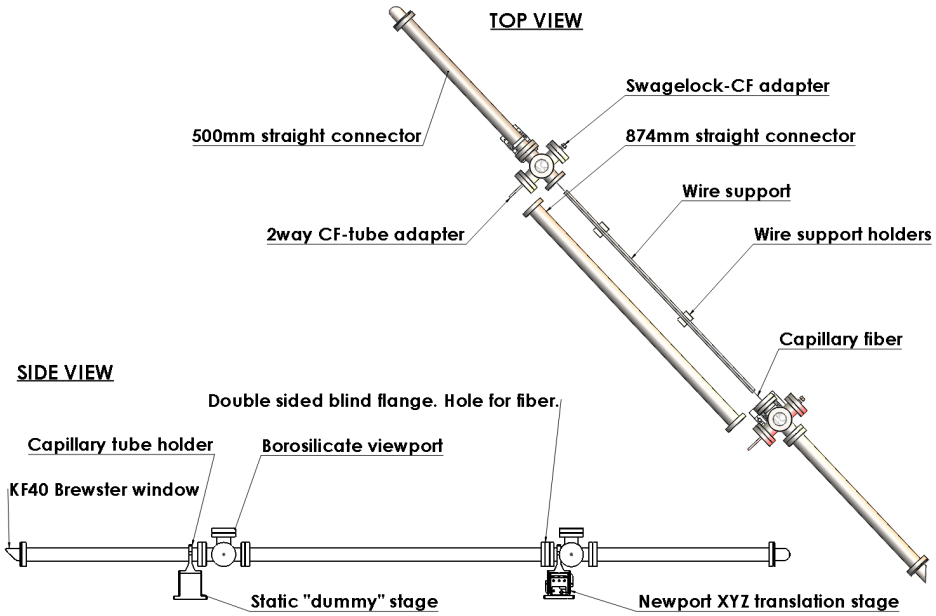

Figure 10: More detailed schematic of the HCF pressure chamber.

case damage the windows.

The 500 mm straight connectors are each connected to a 5-way connector, which enables gas inlets and outlets. The 5-way connectors also each have a borosilicate glass viewport in order to visually observe the coupling from either side of the HCF. A 874 mm tube connects the two 5-way connectors, the length is calculated such that the HCF is centered at each of the 5-way connectors.

The entire pressure chamber is mounted on a translation stage and a static "dummy" stage. The dummy stage just fixates the chamber at a certain height and the translation stage allows for redirecting the output of the capillary. The alignment procedure is thus not only restricted to just using mirrors to ensure correcting coupling position and angle.

As the throughput of the HCF is very sensitive to the bending of the capillary, a support is designed in order to ensure that the HCF is straight. The support consists of two metal wires on two half-cylindrical feet. Fig. 11 shows a cross-section of the 874 mm tube with the supports placed inside. The fiber rests on the wires and the indentation in the half-cylindrical feet is measured such that the HCF is in the center of the tube.

Since the HCF is inserted in a blind flange, it is very susceptible to bending if this flange is not assembled perfectly. Rubber "O"-rings are used as insulation between the flange connections as they provide elastic deformation when fastened.

Figure 11: Cross-sectional close up of the HCF wire support.

For ultra-high vacuum, copper gaskets are used to insulate flange connections, as these are plastically deformed they can not be un-tightened without creating an opening to the pressure chamber. Whereas the flange connection angle can be adjusted with the use of rubber "O"-rings.

2.3 Experimental Setup

2.3.1 Optical Parametric Amplification

The pump source for the OPA is a high power Ti:Sapphire laser with an output of 5 mJ pulses centered at 800 nm and a repetition rate of 1 KHz. The pulses have a bandwidth of 100 nm and a duration of 20 fs.

The Ti:Sapphire laser is used to pump a TOPAS (Traveling wave Optical Parametric Amplifier of Super-fluorescence). The TOPAS splits the 800 nm pump beam into an idler and a signal. Both the idler and the signal have lower photon energy than the pump, and by convention the idler is the component with lower energy per photon, and the signal is the component with higher photon energy, see Fig. 12. This splitting can be described as Difference Frequency Generation (DFG). Pump energies up to 5 mJ can be used and the conversion efficiency is up to 30% of the input energy. This 30% conversion efficiency refers to the sum of the signal and idler output.

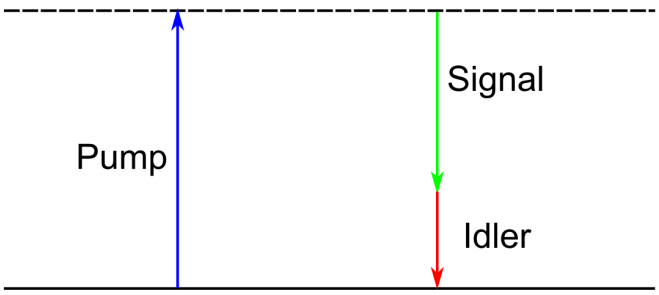

Figure 12: Simple illustration of the down-conversion process.

The OPA process is possible when the second order susceptibility tensor $\chi^{(2)}$ (Eq. 7) is present, meaning that this process only occurs in crystals or other non-isotropic materials. The process shown in Fig. 12 requires phase matching, which is enabled by using birefringent crystals (crystals that have two different indices of refraction).

In order to stimulate this process one needs to in beforehand create the signal in order to mix it with the pump and birefringent crystals that phase match the DFG. Fig. 13 illustrates the pre-amplification phase inside the TOPAS. The input is split by a beam splitter (BS) into a weak beam (pulse energies are in the order of μJ) and a pump beam. The weak signal beam is then sent through a Sapphire plate to create a white light continuum, in a similar to the spectral broadening described in Sec. 2.1.2. The white light is then heavily chirped in a SF_6 glass plate in order to stretch it in time. The pump is then non-collinearly

overlapped with the chirped white light beam in a nonlinear crystal in order to amplify the signal illustrated in Fig. 12. By changing the delay between the pump and the white light signal beam it is possible to choose a narrow spectral part of the white light, thus tuning the signal and the idler wavelength. The signal and pump beam are then overlapped in a phase matched nonlinear crystal. In the TOPAS, the beam is actually split into three pump beams, which means that the last OPA step is repeated one more time with an additional pump beam.

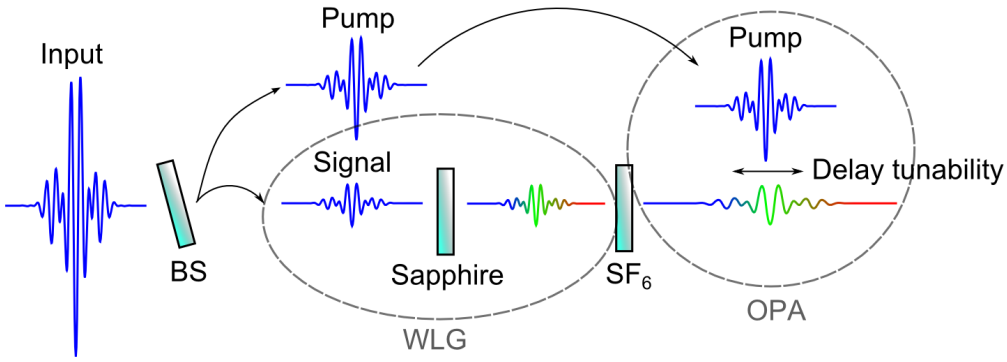

Figure 13: Creation of the TOPAS output.

Using this method of down-converting light it is possible to tune the output of the TOPAS between 1100-2600 nm (signal: 1100-1600 nm, and idler: 1600-2600 nm). However, efficiency is depends on the phase matching angles of the nonlinear crystals, meaning that there is an optimum of the signal and the idler respectively.

A measurement of the TOPAS output can be seen in Table 2, the signal efficiency peaks at around 1300-1400 nm whilst the idler peaks at 1800 nm. As SPM relies on high intensities, the efficiency peak of the signal is chosen for the experiment.

Signal λ [nm]	Signal P [mW]	Idler λ [nm]	Idler P[mW]
1200	450 ± 50	2400	250
1220	520 ± 50	2320	280
1240	560 ± 50	2260	340
1260	700 ± 50	2200	350
1280	710 ± 80	2130	440 ± 30
1300	650 ± 80	2080	400 ± 30
1320	810 ± 50	2030	470 ± 30
1340	780 ± 40	1990	530 ± 10
1360	710 ± 60	1940	560 ± 10
1380	790 ± 60	1900	580 ± 10
1400	810 ± 30	1870	590 ± 5
1420	790 ± 40	1830	580 ± 10
1440	760 ± 60	1800	610 ± 10
1460	660 ± 60	1770	590 ± 10
1480	730 ± 60	1740	570 ± 10
1500	630 ± 70	1710	570 ± 20
1520	550 ± 70	1690	550 ± 20
1540	500 ± 150	1670	400 ± 50
1560	280 ± 230	1640	470 ± 30
1580	300 ± 300	1620	450 ± 100

Table 2: Table showing measured output of the TOPAS at various wavelength configurations for the signal and the idler.

2.3.2 Coupling Into the Hollow Core Fiber

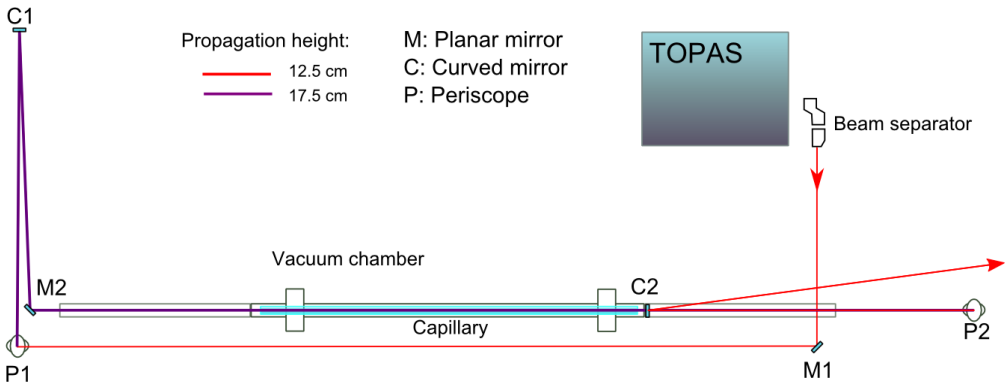

Figure 14: The mirror assembly which directs the beam into the capillary.

In order to direct the beam from the output of the OPA and couple it into the HCF, an experimental setup has to be constructed. In Fig. 14 we see a schematic top view of the beam as it propagates from the TOPAS through the implemented experimental setup. The beam goes through a beam separator in order to separate the signal and the idler. The chamber is placed 17.5 cm above the optical table, allowing for free beam passage below it. Mirror M1 simply directs the beam to the entrance side of the capillary. Periscope P1 elevates the beam to the chamber height. Curved mirror C1 focuses the beam into the HCF and mirror M2 is used direct the beam straight into the HCF. At the output of the chamber, the beam is redirected using a retro-reflecting periscope P2 to the collimating mirror C2.

To achieve efficient coupling into the capillary, the focusing mirror C1 has to be chosen such that the size of the beam waist at the focus is corresponding to 0.64 of the capillary entrance diameter. By choosing such a relation, 98% of the fundamental mode ($EH_{1,1}$) of the light is efficiently coupled into the capillary [29], providing minimal waveguide attenuation according to Eq. 15. This arises from the fact that the wavefront of the beam is planar at the focus, in Gaussian wave optics, and therefore the beam is confined within the HCF when it has very little divergence.

The Helium Neon (He-Ne) laser used for aligning the high power laser beam is coupled from the back side of the capillary using a lens and the retro-reflecting periscope P2. Upon transmission, the 800 nm beam and the TOPAS beam can individually be aligned to the He-Ne in order to couple into the capillary.

We can determine the correct focusing mirror required for optimal coupling by using ray tracing and Gaussian optics. The beam waist and radius of curvature as a function of distance is expressed as [21]:

$$\omega^2(x) = \omega_0^2 \left[1 + \left(\frac{\lambda x}{\pi \omega_0^2}\right)^2\right], \tag{20}$$

$$R(x) = x \left[1 + \left(\frac{\pi \omega_0^2}{\lambda x}\right)^2\right], \tag{21}$$

where $\omega(x)$ is the beam radius in the at the position x, w_0 is the radius at the beam waist. R is the radius of the wavefront and λ is the carrier wavelength of the pulse. These two equations are needed in order to express the complex beam parameter, q, which in turn is required in order to couple Gaussian wave optics to ray transfer matrices:

$$\frac{1}{q(x)} = \frac{1}{R(x)} - \frac{i\lambda}{\pi \omega(x)^2}. \tag{22}$$

The coupled expression for the q parameter after propagation through optical elements is given by.

$$q_f = \frac{Aq_i + B}{Cq_i + D}, \tag{23}$$

where A,B,C and D are the matrix elements of the ray transfer matrix, for the different optical elements which are described in [21].

It is thus possible to calculate the propagation of the beam using ray optics in order to express the system in a ray transfer matrix. The matrix elements are used in order to obtain the complex beam parameter q, which can be used to extract the radius of the wavefront and the beam radius using Eq. 22. Ultimately the beam waist at the focus ω_0 is obtained, and by tuning the size of the beam before propagation through the focusing elements and the curvatures of the focusing elements themselves it is possible to find a solution for a beam waist which is 0.64 of the entrance aperture of the HCF.

For the TOPAS output, the beam diameter is estimated to be 5-6 mm, and has the carrier frequency 1300 nm. Choosing a 1.5 m focusing mirror in order to focus into the HCF entrance yields a beam diameter which is approximately 250 μm. That is, 10% larger than the optimum for coupling in a 350 μm capillary.

3 Results & Discussion

3.1 Design Test

A first design test was conducted in order to determine the straightness of the HCF when it is resting on the support, and in order to determine if the capillary was clean. The fiber was in this test just on the wire supports, in the 874 mm connector, which was resting on the translation stage and the dummy stage. The test would reveal whether the supports or the capillary was defective. The initial results were promising, although a perfect fundamental mode was never achieved, low order modes were consistently achieved with a 80-85% throughput with a helium-neon laser.

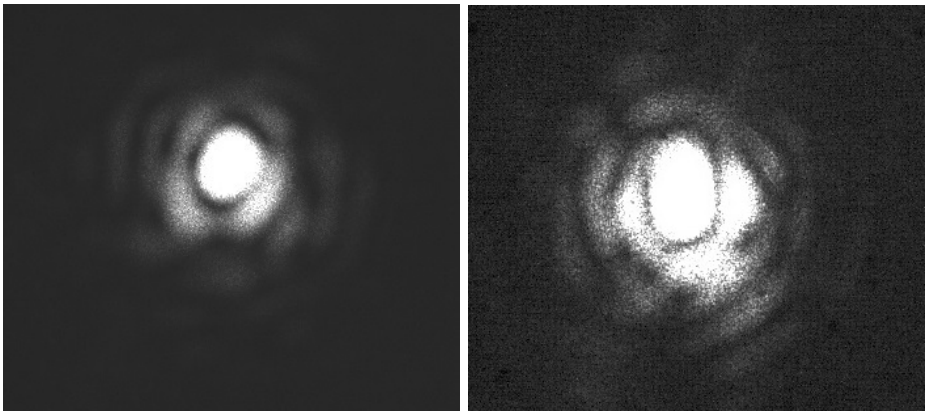

(a) 15% throughput. **(b)** 30% throughput

Figure 15: Monochrome image of the HeNe-laser beam profile after propagation through the capillary. The power is measured directly after observing mode structure. These are the two best modes in the first attempt at obtaining good transmission and modal structure using the fully assembled chamber. Figure **a** demonstrates a decent and symmetric looking mode, although the transmission is too low.

As the chamber then was fully assembled, a first test revealed that both mode quality and throughput was drastically reduced. In Fig. 15 we see reasonable mode structure but very low throughput. The reason for the high attenuation were assumed to be due to deformation of the capillary.

After an rigorous error scan it was determined that the error was introduced in either one or several of three possible places. Either the wires which support the fiber, the blind flange that separates the two pressure chambers, or simply due to the fact that the fiber is hanging under of its own weight in the high pressure compartment where it is not supported.

Each of these errors were accounted for, a small support was created and placed

at the point where the fiber was assumed to have most bending. The wire supports were smoothed at the point where they previously had been cut, as there were metal splinters protruding at this point. And finally, the blind flange (which was intended for differential pumping) was removed. Instead, the chamber would be over pressurized with no differential pumping. Despite this, the throughput with the He-Ne laser never reached more than 50% throughput. The reason this reduction was that, as opposed to the first test, the beam cannot be traced after it has entered the 500 mm connectors. This means that optical evaluation of the focus and direction is done half a meter before the He-Ne is coupled into the capillary.

3.2 800 nm Experiment

The first experiment with the aim of spectral broadening was conducted with the 800 nm laser. Such an experiment would show if it was possible to align a high power laser to the He-Ne laser in this current setup. Also it is much easier to broaden with the 800 nm laser, since it has more power than the TOPAS. As the 800 nm is readily used for broadening in another capillary, it would also indicate whether problems with coupling high power laser are due to the focusing optics, or if they arise when we use the TOPAS.

The results of this proved promising. As for pure waveguide attenuation it was possible to achieve close to 50% throughput of 800 mW of the 800 nm laser despite having the wrong focusing mirror into the capillary (since it was chosen to fit the TOPAS beam). Furthermore, the size of the 800 nm beam had to be reduced in size in order not to focus too hard for when coupling into the capillary. The reduction was achieved using a simple iris. However, the iris gave rise to a ring pattern in the beam which was to be focused, which might have introduced focusing errors.

Fig. 16 shows the spectrum of the 800 nm laser after propagation through the HCF when the chamber is filled with argon. The throughput of the HCF without gas is approximately 50%, the input pulse energy is 0.8 mJ after trimming the beam spot with the iris. Attenuation due to ionization is however notable, at 0.5 Bar the intensity is approximately the same for 0 Bar, at 1 Bar the half the intensity lost due to ionization of the gas.

The broadening is noticeably increasing with pressure. At 0 Bar the pulses have a 100 nm FWHM wavelength bandwidth, at 0.5 Bar it is 150 nm and at 1 bar approximately 225 nm. However, an increase of a factor two of the wavelength bandwidth in this case is not a favorable trade for a 75% loss.

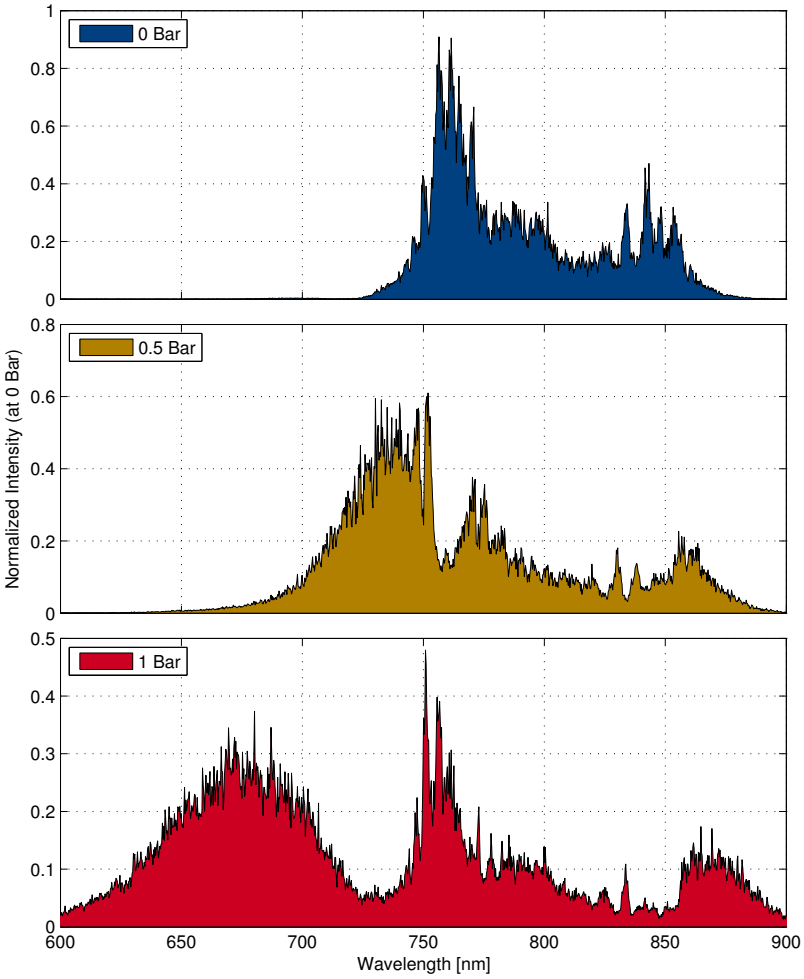

Figure 16: The spectrum observed after propagation through Argon. At 0.5 Bar the losses are fairly low. At 1 bar, the losses are close to 50% of the input intensity.

Even though the results from Fig. 16 indicate good spectral broadening in argon, the shape of the spectrum might also be modulated due to the loss of intensity. Fig. 17 shows the same experiment, but conducted in neon. As neon has a higher ionization potential than argon, the pressure can be increased much more until ionization losses become prominent. As a matter of fact, information regarding ionization losses is extinguished by the fluctuations in the (fairly) stable spectra seen in Fig. 17. The broadening seen in neon is smaller, despite having twice as high pressure and throughput as compared to argon. The broadening is still just slightly more than half of that seen in argon. This trend is, without any quantitative analysis in good agreement with the relative size of the susceptibilities of argon and neon from Eqs. 18,19.

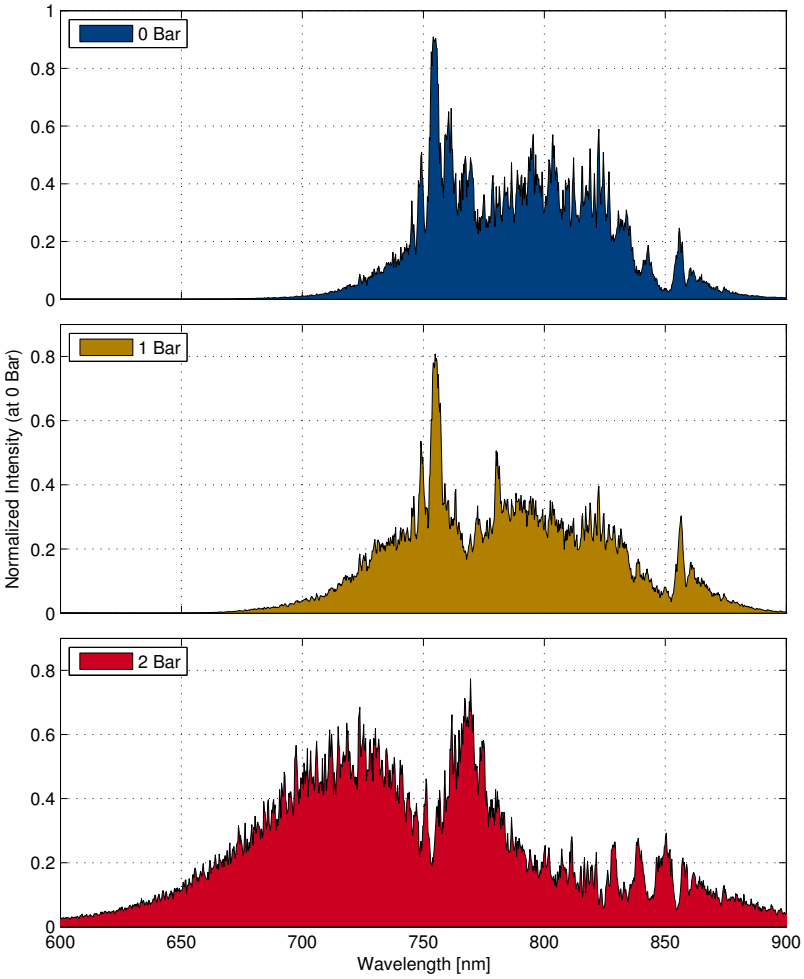

Figure 17: The spectrum observed after propagation through Neon. Again, the fluctuations made it impossible to determine with any decent precision what the losses are. However, it is possible to discern that the throughput is pretty much similar for all pressures.

3.3 TOPAS Experiment

Once the TOPAS was aligned and tuned, it was realized that the beam spot size was much smaller than earlier estimations, approximately 2 mm in diameter. In order to achieve efficient focusing it was determined that the beam ought to be enlarged using a telescope. Furthermore, as the TOPAS is much less energetic than the 800 nm laser, it was decided to have a translation stage for a retro-reflecting setup of the focusing mirror. Such a translation stage would allow for efficient placement of the focus, without changing the coupling angle of the beam into the HCF.

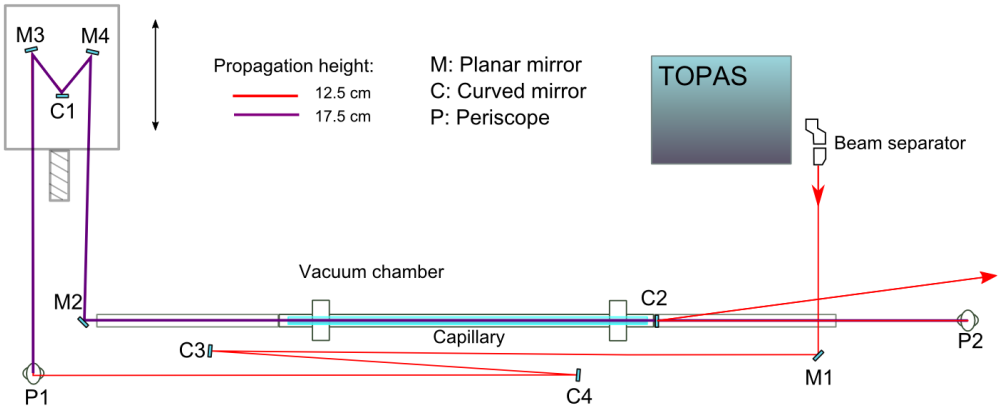

Figure 18: Improved mirror setup used for coupling into the HCF.

Fig. 18 shows the new mirror setup. C3 and C4 is a set consisting of an expanding mirror and a collimating mirror. The magnification of the telescope is a factor 3, which ultimately would provide a 6 mm beam diameter. Mirror M3, M4 and C1 are now placed on a linear translation stage. Provided that the beams coming from P1 and going to M2 are parallel, the incidence angle of the beam into the capillary will not change as the position of the focus is moved.

As this addition of mirrors introduces more reflection losses, the signal beam becomes quite weak before coupling into the capillary. A power measurement revealed that 0.35 mJ of the beam is sent into the HCF chamber, the throughput was only 0.05 mJ.

Nonetheless, spectral broadening was achievable using at these low pulse energies. In Fig. 19 the spectrum after propagation through argon in the HCF is shown for different pressures. The loss of energy in this case does not come from ionization, but rather due to the coupling into the HCF. The retro-reflecting focusing mirror stage was not perfectly designed, and thus the coupling had to be tweaked for each pressure. Despite the low energies, the spectrum is broadened almost by a factor of two, of course depending on how the observer chooses to

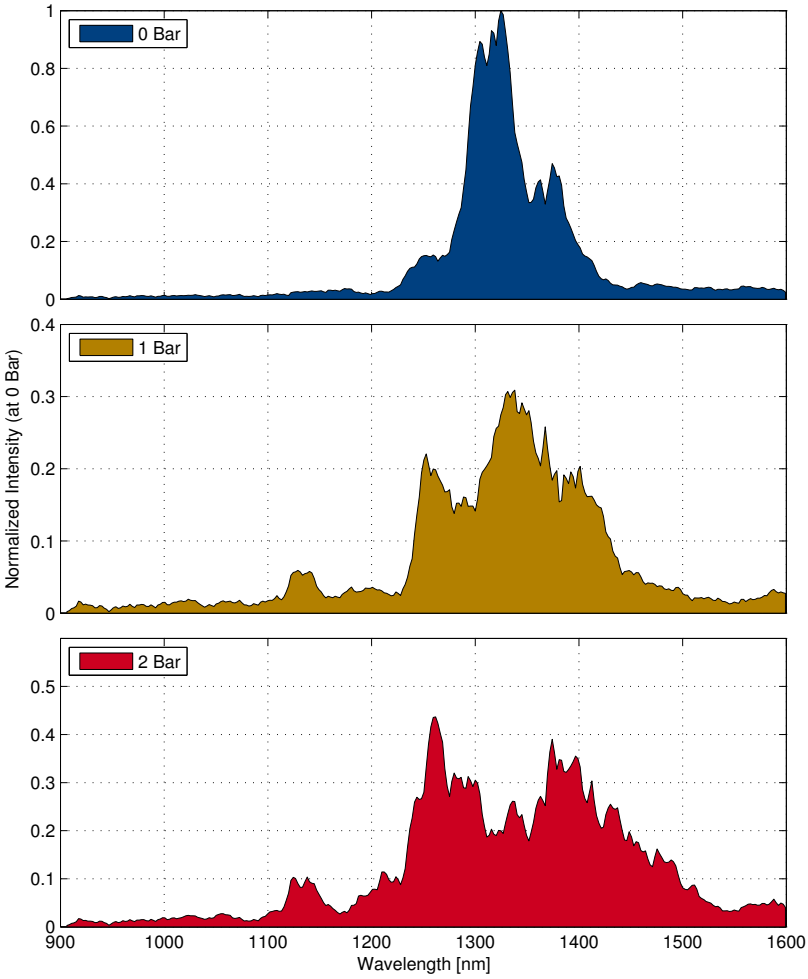

Figure 19: Argon pressure scan of the TOPAS output. Signal centered original signal centered around 1340 nm.

define the FWHM of the pulse. But even in absolute terms, we see that there are new spectral components created in the chamber.

Fig. 20 shows the output spectrum for when the TOPAS is tuned to 1400 nm. This time, the the coupling was more successful between the increases in pressure, part of this success might be attributed to the fact that the beam was over-expanded in the telescope, likely to the point where the beam waist was too small for the 1300 nm beam. The input pulse in this case is very broad to start with, which remarkably leads to a very large bandwidth once spectrally broadened in the HCF.

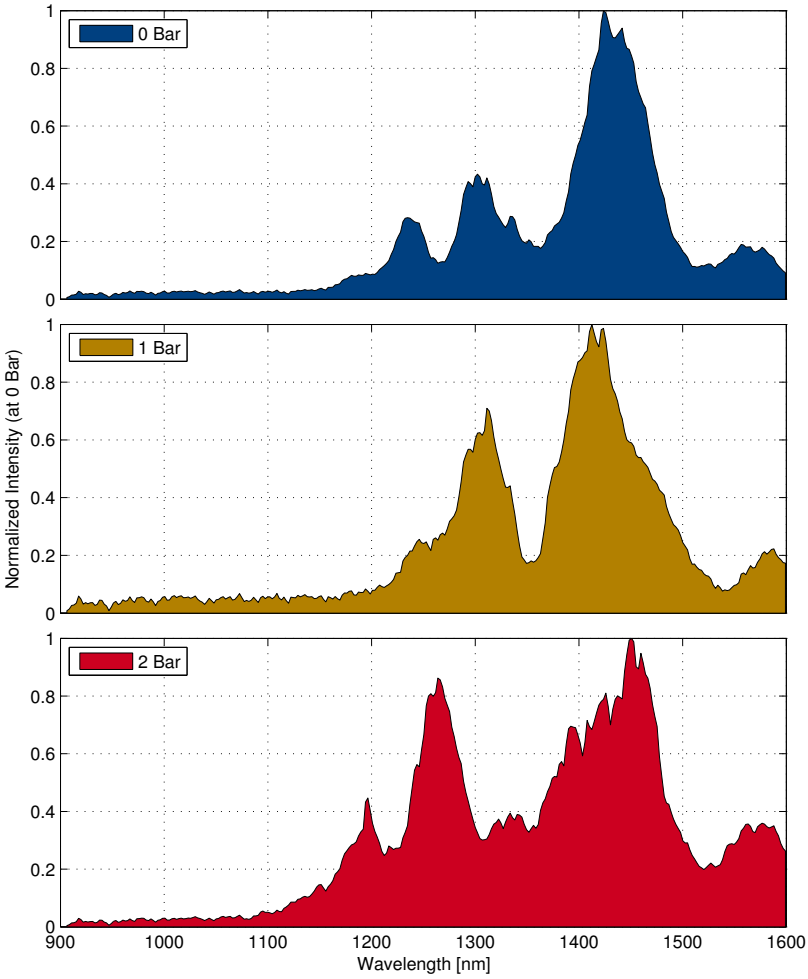

Figure 20: Pressure scan of the TOPAS output. Original signal centered around 1400 nm.

A more interesting approach to achieve broadening is to utilize the increase of the third order susceptibility, $\chi^{(3)}$, when the carrier wavelength is close to resonance [30]. As noble gases do not form a molecular gas, the closest resonance is always in the ultraviolet. However, the water in air (or specifically the hydroxide) contains a resonance close to 1400 nm [31], which in practice could be utilized in order to broaden the pulse.

Fig. 21 shows a measurement conducted in air. As the source of air is not supplied from a compressor, the highest attainable pressure in the chamber is one atmospheric pressure. This proves to be insufficient in order to broaden the weak pulses supplied by the TOPAS.

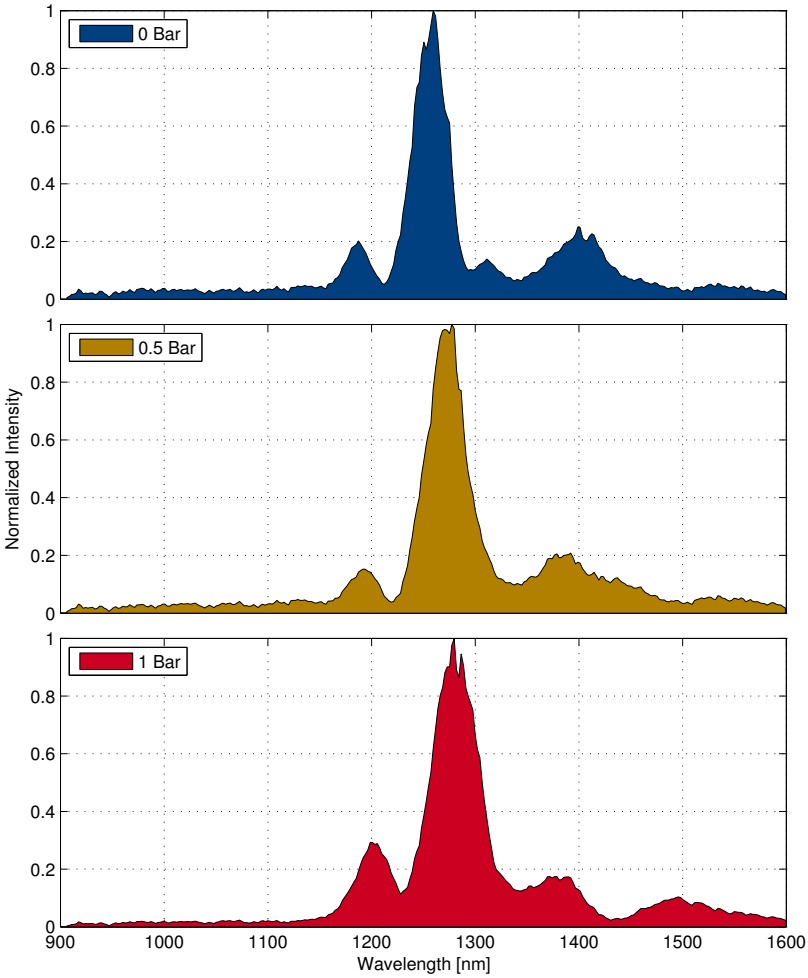

Figure 21: Output after propagation through HCF filled with air.

4 Conclusions & Outlook

From the experiments presented in Sec. 3.3 it is apparent that it is possible to spectrally broaden even a weak signal beam from the TOPAS in a gas filled HCF. The largest bandwidth achieved for a pulse with a carrier wavelength in the short wavelength infrared is approximately 300 nm, which would provide a transform limit corresponding to the duration of four optical cycles. The throughput in all the TOPAS experiments is too low in order to conduct any HHG experiments, and further efforts have to be invested into obtaining the correct beam spot size and correct coupling into the HCF.

Broadening in a molecular gas might prove promising despite the lack of spectral broadening presented in 21, as the actual resonance is closer to 1400 nm than 1300 nm. Preferably a wavelength scan should be performed around the hydroxide resonance in air in order to determine if there is a possibility of achieving better SPM than in noble gases. It would also be favorable to compress air into the chamber in order to have a higher third order nonlinear susceptibility $\chi^{(3)}$.

Besides from having a low throughput, the output of the HCF is fluctuating a lot. All of the spectra from Sec. 3.3 are integrated over seconds and then averaged 30 times, in order to obtain a stable spectrometer reading. The signal beam of the TOPAS is accompanied by parasitic beams in the visible to Near Infrared (NIR) regime, these are created due to various $\chi^{(2)}$ processes in the TOPAS. These are however helpful, since they can be visually examined on a flourescent paper. As they are broadened in the HCF they will appear as flashing white light on the paper. The fluctuation of this white flashing is consistent with the appearance of spectral broadening of the short wavelength infrared spectrum on the spectrometer. It is still not known if these fluctuations are associated with air turbulence in the beam-line, or if it is caused by vibrations of the optical elements in the setup.

It is possible that the fluctuations are introduced in the TOPAS, and it would be useful to investigate the beam stability before and after the TOPAS. Provided that the fluctuations are introduced after the TOPAS, then the stability should be investigated after each optical element. If such a scan would prove inconclusive, then one could assume that the fluctuations are introduced due to turbulence, and this can be solved by better enclosing the beamline.

In the end, the single largest problem in the setup in order to obtain good throughput is the coupling. The best method of obtaining better coupling is to fix the differential pumping, which would solve the problem of having a pressure dependent focal position at the HCF entrance, and also eliminate any potential nonlinear focusing effects. The differential pumping would also remove two mirrors from the setup, reducing the reflection losses which arise even before the

coupling into the HCF.

An alternative, which might solve many of the aforementioned problems ,would be to utilize the self-focusing effect mentioned in Sec. 2.2.2 in order to use filamentation as a waveguide [32]. Filamentation provides very low attenuation and is very insensitive to the stability defects which cause a destructive coupling efficiency. In a comparative experiment conducted it is stated that it is possible to almost obtain twice as much throughput using a filamentation waveguide as compared to propagation through a HCF [33]. However, the phase which is introduced from filamentation might be more complex than that acquired in a HCF, as tighter focusing has to be introduced in order to confine a beam through filamentation, which leads to more ionization. The chirp introduced using filamentation might not be as compressable as that from broadening in a HCF. The broadening achieved by using filamentation as a waveguide is also significantly less, still, it would not require a large change in the current setup in order to attempt broadening using filamentation.

The KDP crystal needed in order to compress the pulses has to be acquired, and the pulse has to be characterized in order to determine if compression is possible using the KDP. The planned methods for determining the duration are Frequency Resolved Optical Gating (FROG) [34], and the D-scan technique presented in [35].

5 Acknowledgements

During my time in the Attosecond Group in the Department of Atomic Physics in Lund I have been fortunate to work with people who are more than eager to share of their knowledge with me. I owe the bulk of my gratitude to Johan Mauritsson for accepting me both as a bachelor student, and later, a master student. Equally much I have to thank Esben Witting Larsen for supervising me during both of these projects and providing help and guidance.

I wish to thank Samuel Bengtsson who, of his own free will, aided me in my experiments and provided invaluable, helpful discussions. I owe many thanks to Cord Arnold for sharing with his professional experience regarding pulse compression and capillary chamber assembly and Hampus Wikmark for help with physically assembling my chamber and good office company.

In the end, I cannot think of a single person in the Attosecond Group which has not contributed to my thesis and workplace experience in any way. That is why I would like to extend my gratitude to everyone in this group, and express my best wishes to each and every person.

References

[1] http://www.lightcon.com/products/product.php?ID=152

[2] Bruno E. Schmidt *et. al.*, *Compression of 1.8 μm laser pulses to sub two optical cycles with bulk material.* APPLIED PHYSICS LETTERS 96, (2010).

[3] G.Gordon, W.M. Cady, *An Apparatus for Time-Resolved Spectroscopy* JOSA, Vol. 40, Issue 12. 1950.

[4] T.H. Maiman. *Stimulated Optical Radiation in Ruby.* Nature, VOL. 187, (1960).

[5] F.J. McClung & R.W. Hellwarth, *Giant Optical Pulsations from Ruby*, JOURNAL OF APPLIED PHYSICS 33. (1962).

[6] L.E. Hargrove *et al.*, *Locking of He-Ne laser modes induced by synchronous intracavity modulation.* APPLIED PHYSICS LETTERS 5, (1964).

[7] A. H. Zewail, *Laser Femtochemistry* SCIENCE, VOL. 242. (1988)

[8] http://www.nobelprize.org/nobel_prizes/chemistry/laureates/1999/press.html

[9] A. McPhearson *et al.*, *Studies of multiphoton production of vacuum-ultraviolet radiation in the rare gases.* JOSA B. VOL 4. (1987)

[10] A. L'Huillier, P. Balcou. *High-order harmonic generation in rare gases with a 1-ps 1053-nm laser.* PHYSICAL REVIEW LETTERS, Volume 70, (1993).

[11] P.M. Paul *et al.*, *Observation of a Train of Attosecond Pulses from High Harmonic Generation.* SCIENCE, 1 June, 20

[12] P.B. Corkum, *Plasma perspective on strong-field multiphoton ionization.* PHYSICAL REVIEW Volume 71, (199

[13] Kenichi L. Ishikawa. *High-Harmonic Generation, Advances in Solid State Lasers Development and Applications*, Mikhail Grishin (Ed.). (2010)

3).

[14] J. Mauritsson. *Temporal Aspects of High-Intensity Laser-Matter Interactions.* Ph.D. Thesis. Lund University: Sweden, (2003).

[15] J.L. Krause *et al.*, *High-Order Harmonic Generation From Atoms and Ions in the High Intensity Regime.* PHYSICAL REVIEW LETTERS Volume 68, (1992).

[16] B. Shan & Z. Chang, *Dramatic extension of the high-order harmonic cutoff by using a long-wavelength driving field.* PHYSICAL REVIEW Volume 65, (2001).

[17] A.D. Shiner *et al.*, *Wavelength Scaling of High Harmonic Generation Efficiency* PHYSICAL REVIEW LETTERS Volume 103, (2009).

[18] Giguere. M. *et al.*, *Pulse compression of submillijoule few-optical-cycle infrared laser pulses using chirped mirrors.* OPTICS LETTERS Volume 34, 2009.

[19] Harimoto. T., Yamakawa. K. *Self compression of Yb-doped solid-state lasers by combination of self-phase modulation and group-velocity dispersion in KDP crystal.* OPTICS EXPRESS Volume 15, 2007.

[20] F.Mitschke. *Fiber Optics.* Berlin, Heidelberg: Springer Berlin Heidelberg, (2010).

[21] B.E.A. Saleh, M.C. Teich. *Fundamentals of Photonics.* Hoboken,N.J.: Wiley-Interscience, (2007).

[22] J.C. Diels. *Ultrashort Laser Pulse Phenomena.* Amsterdan; Boston: Elsevier/Academic Press, (2006).

[23] A.Korpel. *Split-step-type angular plane-wave spectrum method for the study of self-refractive effects in nonlinear wave propagation.* JOSA B. VOL 3. (1986).

[24] R. W. Boyd. *Nonlinear Optics.* Burlington: Academic Press, (2008).

[25] G.P. Agrawal. *Nonlinear Fiber Optics.* San Diego: Academic Press, (2007)

[26] A. E. J. Marcatili and R. A. Schmeltzer. *Hollow metallic and dielectric waveguides for long distance optical transmission and lasers.* The bell system technical journal, 43(4), July 1964.

[27] H.J. Lehmeier *et. al. Nonresonant third order hyperpolarizability of rare gases and* N_2 *determined by third harmonic generation.* OPTICS COMMUNICATIONS Volume 56, No. 1, 1985.

[28] R.Y. Chiao *et. al. Self-Trapping of Optical Beams* PHYSICAL REVIEW LETTERS Volume 13, (1964).

[29] Angelo Sampaolo *et. al. Single mode operation with mid-IR hollow fibers in the range 5.1-10.5* μm. OPTICS EXPRESS Volume 23, No. 1, (2015).

[30] R.Miles, S. Harris. *Optical Third-Harmonic Generation in Alkali Metal Vapors* Quantum Electronics Volume 9, (1973).

[31] L.S. Grattan, B.T. Meggitt. *Optical Fiber Sensor Technology* Springer US, (2010).

[32] C.P. Hauri, *et. al. Generation of intense, carrier-envelope phase-locked few-cycle laser pulses through filamentation.* Applied Physics B Volume 79, (2001).

[33] L. Gallmann, *et. al.. Comparison of filamentation and the hollow-core fiber characteristics for pulse compression into the few-cycle regime.* Applied Physics B Volume 86, (2007).

[34] D. J. Kane, R. Trebino. *Characterization of Arbitrary Femtosecond Pulses Using Frequency-Resolved Optical Gating.* Quantum Electronics Volume 29, (1993).

[35] M. Miranda, *et. al.. Simultaneous compression and characterization of ultra-short laser pulses using chirped mirrors and glass wedges.* OPTICS EXPRESS Volume 20, No. 1, (2011).